

Article

# Heat Transfer and Dissipation Effects in the Flow of a Drilling Fluid

Wei-Tao Wu <sup>1</sup> and Mehrdad Massoudi <sup>2,\*</sup>

<sup>1</sup> Department of Biomedical Engineering, Carnegie Mellon University, Pittsburgh, PA 15213, USA; weitaow@andrew.cmu.edu

<sup>2</sup> U.S. Department of Energy, National Energy Technology Laboratory (NETL), 626 Cochrans Mill Road, P.O. Box 10940, Pittsburgh, PA 15236, USA

\* Correspondence: mehrdad.massoudi@netl.doe.gov; Tel.: +1-412-386-4975; Fax: +1-412-386-5870

Academic Editors: Goodarz Ahmadi and Bekir S. Yilbas

Received: 29 December 2015; Accepted: 17 March 2016; Published: 18 March 2016

**Abstract:** In this paper we study the effects of dissipation in the Couette flow and heat transfer in a drilling fluid, and explore the effects of concentration and the shear-rate and temperature-dependent viscosity, along with a variable thermal conductivity. A brief discussion on the constitutive relations for the stress tensor, the diffusive particle flux vector, and the heat flux vector is presented. The one-dimensional forms of the governing equations are solved numerically and the results are presented through a parametric study by varying the dimensionless numbers.

**Keywords:** drilling mud; drilling fluid; non-Newtonian fluids; suspension; rheology; variable viscosity; viscous dissipation

**PACS:** J0101

## 1. Introduction

Flow of mixtures composed of solid particles of various shapes and sizes dispersed in a fluid occurs in many industrial processes as well as in nature (see [1,2]). Examples of such complex fluid mixtures are coal slurries and drilling fluids. Drilling fluids are generally water-based or oil/polymer-based. In the formulation of either the water-based or the oil-based drilling fluids several additives are added to maintain proper rheological properties. These additives, and the fact that drilling fluids are composed of mud, pieces of rocks, water, oil, bubble, *etc.*, make the drilling fluid behave as complex non-Newtonian fluids. Flow of these fluids becomes even more complicated during the drilling operation as continuously drill cuts of different size, shape, concentration, pH, *etc.*, are added into the drilling fluids. Amongst the most important properties of the drilling fluid one can name density, viscosity, yield stress, *etc.* When the drilling fluid is subjected to high temperature and high pressure then ionic mobility, reactivity, solubility *etc.*, are increased and these, in turn, change the rheological properties of the drilling fluid. The drilling operation is quite often, as a temporary solution, suspended in order to change the drill bit, to clean the pipe or whenever some other difficulties are encountered. During this stage, the drilling fluid should have the capability of holding the rock cuttings in suspended form and prevent them from settling down in the well annulus (see [3]). Our main interest in this paper is to study the behavior of non-linear fluids which in many ways resemble and behave similarly to drilling fluids.

The success of the drilling operation depends, to a large extent, on variables such as the drill bit design, the selection of the drilling fluid, the climate conditions, the geophysical properties of the ground rock material, *etc.* [4]. The role of the drilling fluid is considered by many researchers to be a prominent one [5]. Hole cleaning is an important issue in the drilling operation, especially in cases of

horizontal drilling, as mentioned by Caenn, *et al.* [6]. Siginer and Bakhtiyavou [7] indicate that the effect of the eccentricity of pipe on the flow of well bore fluids should also be studied. For deep drilling applications, in addition to external factors such as temperature and pressure, factors such as the permeability and deformation properties of the rocks and mudrock instability should be considered [8]. Hole cleaning is related to the ability of the drilling fluid to transport and suspend drilled cuttings. Hole cleaning depends on many variables including well bore inclination, cuttings slip velocity, flow regime, rotary speed of the drill pipe, fluid rheology, flow rate, rate of penetration, cuttings size and shape, wellbore geometry, cuttings density, cuttings agglomeration, the fluid density, the wellbore geometry, pipe rotation, *etc.* [9].

In most drilling applications, the Bingham or the Power-law models are used to represent the drilling fluid behavior (see [10]). However, many drilling fluids behave according to the modified Power-law or the Herschel-Buckley rheological model (see [10]). The shear rate is low in the annulus, and as it is well known, in the low shear-rate regime, that the Power-law model underestimates while the Bingham plastic model overestimates the frictional pressure drops. The Herschel-Buckley model perhaps presents a more adequate constitutive relation [11]. Slawomrski [12], indicated that even though the Bingham plastic model is often used in modeling the drilling fluids, some studies have shown that many of the drilling fluids are non-linear fluids with memory. Briscoe *et al.* [13] indicate that in a high pressure and high temperature environment, the yield stress and the plastic viscosity of the muds are also influenced by pressure and temperature. In many ways, a drilling fluid, when modeled as a (single component) suspension, behaves as a non-linear fluid similar to a slurry where the effects of shear rate and concentration are to be included in the constitutive relation for the stress tensor.

The objective of the present paper is to numerically study the effects of viscous dissipation in the Couette flow and heat transfer in such a fluid, and explore the effects of concentration and the shear rate and temperature-dependent viscosity, along with a variable thermal conductivity. We assume that the viscosity of this non-linear fluid depends on the shear rate and the volume fraction of the particles. The effects of the particle concentration (volume fraction) and its behavior is governed by a convection-diffusion equation. In the next section, the governing equations of motion are provided. Section 3 focuses on the constitutive relations for the stress tensor, the diffusive particle flux vector, and the heat flux vector. In Section 4, we describe the geometry of the problem and provide the derivation for the one-dimensional form of the governing equations, as well as the boundary conditions. In Section 5, we outline the numerical scheme we have used. In Section 6, we perform a parametric study using the different dimensionless numbers.

## 2. Governing Equations

If the drilling fluid is treated as a single component material, in the absence of any electro-magnetic effects, the governing equations of motion are the conservations of mass, linear momentum, angular momentum, concentration and the energy equation. If the drilling fluid is modeled as a multi-component material, then we need to provide the governing equations for all the components, and a multi-phase approach should be used; this requires not only constitutive relations for each component, but also for the interactions among the components [2,14,15]. In this paper, we assume that the drilling fluid can be treated as a single component non-homogeneous fluid. As a result, the governing equations are:

Conservation of mass

$$\frac{\partial \rho}{\partial t} + \text{div}(\rho \mathbf{v}) = 0 \quad (1)$$

where  $\rho$  is the density of the fluid,  $\partial/\partial t$  is the partial derivative with respect to time, and  $\mathbf{v}$  is the velocity vector. For an isochoric motion we have  $\text{div} \mathbf{v} = 0$ .

Conservation of linear momentum

$$\rho \frac{d\mathbf{v}}{dt} = \text{div} \mathbf{T} + \rho \mathbf{b} \quad (2)$$

where  $\mathbf{b}$  is the body force vector,  $\mathbf{T}$  is the Cauchy stress tensor, and  $d/dt$  is the total time derivative, given by  $d(\cdot) / dt = \partial(\cdot) / \partial t + [\text{grad}(\cdot)] \mathbf{v}$ . The conservation of angular momentum indicates that in the absence of couple stresses the stress tensor is symmetric, that is,  $\mathbf{T} = \mathbf{T}^T$ .

In suspension flows, the particle concentration is, in general, not constant and in many applications, it is necessary to have an additional equation, often called the convection-diffusion equation. Here we use the particle concentration equation for  $\phi$  as discussed in [16], based on [17].

Conservation of concentration

$$\frac{\partial \phi}{\partial t} + \mathbf{v}_i \frac{\partial \phi}{\partial x_i} = -\text{div} \mathbf{N} \tag{3}$$

The first term on the left-hand side denotes the rate of accumulation of particles, the second term denotes the convected particle flux (where  $\frac{\partial \phi}{\partial x_i}$  denotes the gradient of the concentration), and the term on the right side denotes diffusive particle flux. Following [17], the diffusive particle flux  $\mathbf{N}$  is composed of fluxes related to the Brownian motion, the variation of interaction frequency and the viscosity.

Conservation of Energy:

$$\rho \frac{d\varepsilon}{dt} = \mathbf{T} : \mathbf{L} - \text{div} \mathbf{q} + \rho r_1 \tag{4}$$

where  $\varepsilon$  is the specific internal energy,  $\mathbf{L}$  is the gradient of velocity,  $\mathbf{q}$  is the heat flux vector,  $r_1$  is the specific radiant energy, and “:” designates the scalar product of two tensors. Thermodynamical considerations require the application of the second law of thermodynamics or the entropy inequality. The local form of the entropy inequality is given by (see [18], p. 130):

$$\rho \dot{\eta} + \text{div} \varphi - \rho s \geq 0 \tag{5}$$

where  $\eta(x, t)$  is the specific entropy density, the dot implies the material time derivative,  $\varphi(x, t)$  is the entropy flux, and  $s$  is the entropy supply density. If it is assumed that  $\varphi = \frac{\mathbf{q}}{\theta}$ , and  $s = \frac{r}{\theta}$ , where  $\theta$  is the absolute temperature, then Equation (5) reduces to the Clausius-Duhem inequality:

$$\rho \dot{\eta} + \text{div} \frac{\mathbf{q}}{\theta} - \rho \frac{r}{\theta} \geq 0 \tag{6}$$

In this paper, we do not consider the consequences of the Clausius-Duhem inequality [18–21]. In the next section, we will address the constitutive relations for the stress tensor, the heat flux vector  $\mathbf{q}$  and the diffusive particle flux  $\mathbf{N}$ .

### 3. Constitutive Equations

Drilling fluids are complex multi-component fluids; in general, a drilling fluid is composed of water, oil, pieces of rocks, sand, mud, *etc.*, with bubbles and other chemicals added to this mixture for various reasons. Most researchers assume that a drilling fluid is a suspension whose rheological properties can be described using a non-linear (non-Newtonian) fluid. Based on the available experimental observations, drilling fluids exhibit characteristics similar to those of non-linear materials, such as colloidal suspensions, polymers, rubber, slag, *etc.* For complex materials, the main points of departure from linear behavior are: (1) The ability to shear thin or shear thicken; (2) The ability to creep; (3) The ability to relax stresses; (4) The presence of normal stress differences in simple shear flows; (5) The presence of yield stress; (6) Memory effects, *etc.* For many practical fluid engineering applications, the viscosity may be a function of time, shear rate, concentration, temperature, pressure, electric field, magnetic field, *etc.* Therefore, in general,  $\mu = \mu(t, \Pi, \theta, \phi, p, \mathbf{E}, \mathbf{B})$ , where  $t$  is the time,  $\Pi$  is some measure of the shear rate,  $\theta$  is temperature,  $\phi$  is concentration,  $p$  is pressure,  $\mathbf{E}$  is the electric

field, and  $\mathbf{B}$  is the magnetic field. For some materials or some applications, the dependence of one or more of these can be dropped (see [22]).

### 3.1. Stress Tensor

A general constitutive relation for stress tensor of the drilling fluid should at the very least be able to predict (or include) some type of yield stress and a viscous stress with shear-thinning capabilities, *i.e.*, where the coefficient of viscosity depends on the shear rate. Thus, we assume:

$$\mathbf{T} = \mathbf{T}_y + \mathbf{T}_v \tag{7}$$

where  $\mathbf{T}_y$  is the yield stress and  $\mathbf{T}_v$  is the viscous stress. In general, the yield stress can be obtained from experiments and for the viscous stresses a model is needed where the shear viscosity depends on volume fraction, temperature, pressure, chemical composition and the shear rate. In this paper, we will not include the yield stress (In our next study, we plan to model and study the yield stress part of the stress tensor.) in our model and we only consider the viscous stress which we assume to be given by a generalized Power-law fluid model:

$$\mathbf{T}_v = -p\mathbf{1} + \left[ \mu_r \left( 1 - \frac{\phi}{\phi_{max}} \right)^{-\beta} e^{\alpha(\theta_0 - \theta)} \right] \Pi \frac{m}{2} \mathbf{D} \tag{8}$$

$$\Pi = 2tr\mathbf{D}^2 \tag{9}$$

$$\mathbf{D} = \frac{1}{2} (\mathbf{L} + \mathbf{L}^T) \tag{10}$$

$$\mathbf{L} = grad\mathbf{v} \tag{11}$$

where  $\mu_r$  is the reference viscosity,  $\phi_m$  is the maximum volume fraction at which the suspension exhibits fluid behavior,  $\beta$  is an experimentally determined coefficient,  $\theta_0$  and  $\mu_0$  are reference values, and  $\alpha$  is a constant. Here,  $\mathbf{1}$  is the identity tensor,  $p$  is the pressure,  $\theta$  is temperature,  $\phi$  is the volume fraction (The function  $\phi$  is an independent kinematical variable called the volume distribution or volume fraction function (related to concentration) having the property  $0 \leq \phi(x, t) \leq \phi_{max} < 1$ . The function  $\phi$  is represented as a continuous function of position and time; in reality,  $\phi$  in such a system is either one or zero at any position and time, depending on whether one is pointing to a particle or to the void space (fluid) at that location. Now,  $\rho$ , is related to  $\rho_f$  (density of pure fluid) and  $\phi$  through  $\rho = (1 - \phi) \rho_f$ .),  $tr$  is the trace operator,  $\Pi$  is an invariant of  $\mathbf{D}$  where  $\mathbf{D}$  is the symmetric part of the velocity gradient,  $\mu$  and  $\Pi$  together form the effective viscosity, and  $m$  is a material parameter. When  $m < 0$ , the fluid is shear thinning, and if  $m > 0$ , the fluid is shear thickening. For the remainder of this paper, we drop the dependency of  $\mu$  on  $p$ , while recognizing that in many drilling applications, especially in the case of deep-ocean drilling, the effect of pressure should be included (We should mention that the viscosity of drilling muds at high pressure and high temperatures, will also depend on pressure and temperature. For example, Briscoe, *et al.* [13] suggested a high shear-rate viscosity of the type,  $\mu = \mu_0 (1 + \alpha_1(\phi) + \alpha_2(p)p) \exp(E_u + p(B\theta - C)) / k\theta$ , where  $\mu_0$  is a factor related to the activation energy  $E_u$ , the Boltzmann constant ( $k$ ) *etc.*,  $B$  and  $C$  are constants,  $\phi$  is the volume fraction, and  $\alpha_2(p)$  is a compressibility term.). Note that in our previous study, Zhou *et al.* [3], we used a similar but simpler model where the effect of temperature on viscosity was ignored; also, no heat transfer was considered in that paper. In the current model, as shown in Equation (8) which is based on our previous studies, including Gupta and Massoudi [23], Miao *et al.* [24] and Miao and Massoudi [25], we have included an exponentially decaying function for the effects of the temperature. The basic form of the viscosity is based on Krieger's viscosity-concentration correlation ( $\mu = \mu_r (1 - \frac{\phi}{\phi_m})^{-1.82}$ ) [26]. In the model described in Equation (8), we have assumed that the apparent viscosity is not only a function of temperature but also of volume fraction, obeying the Einstein-Roscoe relation [27,28] (if  $\beta = 2.5$ ). It

should be mentioned that alternative ways of modeling non-homogeneous fluids exist (see Massoudi and Vaidya [29,30]).

### 3.2. Heat Flux Vector

According to Fourier [31] (see also Winterton [32]) the heat flux vector depends on the temperature gradient, where

$$\mathbf{q} = -k\nabla\theta \tag{12}$$

and  $k$  is the thermal conductivity of the material. For many complex materials,  $k$  is considered an effective or modified form of the thermal conductivity that depends on concentration, temperature, etc.. In fact, for anisotropic materials,  $k$  becomes a second order tensor. (For a discussion of the effective thermal conductivity concept in porous media and multiphase flows, see [33] (p. 129) and [34–36]). Jeffrey [37] derived an expression for the effective thermal conductivity which includes the second order effects in the volume fraction [38]:

$$k = \kappa_M \left[ 1 + 3\zeta\phi + \hat{\zeta}\phi^2 \right] + O(\phi^3) \tag{13}$$

where

$$\hat{\zeta} = 3\zeta^2 + \frac{3\bar{\zeta}^3}{4} + \frac{9\bar{\zeta}^3}{16} \left( \frac{\omega + 2}{2\omega + 3} \right) + \frac{3\bar{\zeta}^4}{26} + \dots \tag{14}$$

where

$$\zeta = \frac{\omega - 1}{\omega + 2} \tag{15}$$

$$\omega = \frac{k_2}{k_1} \tag{16}$$

where  $\omega$  is the ratio of conductivity of the particle to that of the matrix,  $k$  the effective conductivity of the suspension,  $k_M$  the conductivity of the matrix, and  $\phi$  is the solid volume fraction [34]. More recently, Pabst [39] has derived a relationship for the effective thermal conductivity,

$$k = 1 - \frac{3}{2}\phi + \frac{1}{2}\phi^2 \tag{17}$$

We will use Equations (12)–(16) in this paper. Miao *et al.* [40] used Equation (12) but in their study they assumed that the thermal conductivity is a constant. In this paper, we will consider the case where the thermal conductivity is a function of volume fraction.

### 3.3. Particle Flux

As noted in [16], the various particle fluxes in the concentration equation are due to different mechanisms such as the Brownian motion, sedimentation, particle interactions, etc. In this paper, we assume that the Brownian motion can be neglected and consequently the diffusive particle flux is modeled as:

$$\mathbf{N} = \mathbf{N}_c + \mathbf{N}_\mu \tag{18}$$

where  $\mathbf{N}_c$  is the flux due to particle interactions and  $\mathbf{N}_\mu$  is the flux associated with spatial variations in the viscosity. Based on the proposal of [17], we assume:

$$\mathbf{N}_c = -a^2\phi K_c \nabla(\dot{\gamma}\phi) \tag{19}$$

$$\mathbf{N}_\mu = -a^2\phi^2\dot{\gamma}K_\mu \nabla(\ln\mu) \tag{20}$$

$$\dot{\gamma} = (2\mathbf{D}_{ij}\mathbf{D}_{ij})^{1/2} = (\mathbf{\Pi})^2 \tag{21}$$

where  $a$  is the characteristic particle length (e.g., radius),  $\dot{\gamma}$  is the local shear rate, given by Equation (21),  $\mu$  is the effective viscosity, and  $K_c, K_\mu$  are empirically determined coefficients.

In the next section, we will examine the Couette flow of a fluid modeled as a concentrated suspension where the constitutive relations are given by Equations (8), (13)–(16) and (18)–(20).

#### 4. Couette Flow

For the fully developed Couette flow of a suspension, (shown in Figure 1), we assume:

- (i) the motion is steady;
- (ii) the particle flux due to the Brownian diffusion is neglected;
- (iii) the constitutive equation for the stress tensor is given by Equation (8), the constitutive relation for the particle flux is given by Equations (18)–(20), the constitutive relation for the heat flux is given by Equations (13)–(16).
- (iv) the velocity, the volume fraction, and the temperature profiles are of the form:

$$\begin{cases} v = v(r) e_\theta \\ \phi = \phi(r) \\ \theta = \theta(r) \end{cases} \tag{22}$$

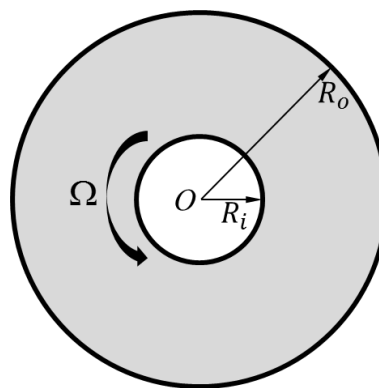


Figure 1. Couette flow.

With Equation (22), the conservation of mass is automatically satisfied, and by substituting Equation (8) into Equation (2), while neglecting the gravity term, the equations of linear momentum reduce to:

$$\begin{cases} \frac{1}{r^2} \frac{d}{dr} \left( r^2 \mu_r \left( 1 - \frac{\phi}{\phi_m} \right)^{-\beta} e^{\alpha(\theta_0 - \theta)} \left| \frac{dv}{dr} \right|^m \frac{dv}{dr} \right) = 0 \\ \frac{dp}{dr} = \frac{dp}{dz} = 0 \end{cases} \tag{23}$$

Substituting Equations (18)–(20) into Equation (3), the concentration equation reduces to

$$\begin{aligned} \frac{K_c}{K_\mu} \left( \phi^2 \frac{d}{dr} \left| \frac{dv}{dr} \right| + \phi \left| \frac{dv}{dr} \right| \frac{d\phi}{dr} \right) + \left| \frac{dv}{dr} \right| \phi^2 \frac{1}{\mu_r \left( 1 - \frac{\phi}{\phi_m} \right)^{-\beta} e^{\alpha(\theta_0 - \theta)} \left| \frac{dv}{dr} \right|^m \frac{d}{dr} [\mu_r \left( 1 - \frac{\phi}{\phi_m} \right)^{-\beta} e^{\alpha(\theta_0 - \theta)} \left| \frac{dv}{dr} \right|^m]} = 0 \end{aligned} \tag{24}$$

Due to the kinematics of the flow, it follows that

$$\frac{d\varepsilon}{dt} = 0 \tag{25}$$

Also, the specific radiant energy,  $r_1$ , is assumed to be negligible. Then the energy equation becomes

$$\mu_r \left(1 - \frac{\phi}{\phi_m}\right)^{-\beta} e^{\alpha(\theta_0 - \theta)} \left| \frac{d\bar{v}}{d\bar{r}} \right|^{m+2} - \frac{1}{r^2} \frac{d}{dr} \left( r^2 k_m (1 + 3\hat{\xi}\phi + \hat{\xi}\phi^2) \frac{d\theta}{dr} \right) = 0 \tag{26}$$

where the first term on the left-hand side is the viscous dissipation (see [41]). Equations (23), (24) and (26) are subject to the following boundary conditions:

$$\left\{ \begin{array}{l} \text{at } r = R_i : v = R_i\Omega = V; \theta = \theta_i \\ \text{at } r = R_o : v = 0; \theta = \theta_0 \end{array} \right. \tag{27}$$

where  $R_i$  and  $R_o$  are the inner and outer radii,  $R_i\Omega$  is the inner wall velocity, and  $\theta_i$  and  $\theta_o$  are the temperature of the inner and the outer walls. Here we assume the no-slip condition for the velocity at the outer wall and a constant velocity at the inner wall;  $\phi$  is the value of the volume fraction, and its value depends to some extent on the average volume fraction  $\phi_{avg}$  through:

$$\phi_{avg} = \frac{2}{R_o^2 - R_i^2} \int_{R_i}^{R_o} \phi r dr \tag{28}$$

We need to assume a value for  $\phi_{avg}$  so that the solution of  $\phi$  can be determined accordingly. If the calculated volume fraction distribution satisfies condition Equation (28), then the original assumption is valid; otherwise a new guess for  $\phi$  must be made until condition Equation (28) is satisfied.

Equations (23) and (24) as well as the boundary conditions, Equation (27), are made dimensionless. The dimensionless quantities are defined as:

$$\bar{v} = \frac{v}{V}, \bar{r} = \frac{r}{R_o}, \bar{\theta} = \frac{\theta - \theta_0}{\theta_i - \theta_0} \tag{29}$$

Substituting Equation (29) into Equation (23) yields:

$$\frac{1}{Re} \frac{1}{\bar{r}^2} \frac{d}{d\bar{r}} \left( \bar{r}^2 \left(1 - \frac{\phi}{\phi_m}\right)^{-\beta} e^{-M\bar{\theta}} \left| \frac{d\bar{v}}{d\bar{r}} \right|^m \frac{d\bar{v}}{d\bar{r}} \right) = 0 \tag{30}$$

Here  $Re$  is the Reynolds number, given by:

$$Re = \frac{\rho VR}{\mu_r}; \text{ and } M = \alpha (\theta_i - \theta_0) \tag{31}$$

For the current problem, due to the kinematics of the flow, that is, the fact that the flow is steady and fully developed, we could have eliminated the  $Re$ . However, we keep the form of the equation as it is for problems involving the pressure gradient term. Substituting Equation (29) into Equations (24) and (26) results in:

$$\begin{aligned} & \frac{K_c}{K_\mu} \left( \phi^2 \frac{d}{d\bar{r}} \left| \frac{d\bar{v}}{d\bar{r}} \right| + \phi \left| \frac{d\bar{v}}{d\bar{r}} \right| \frac{d\phi}{d\bar{r}} \right) \\ & + \left| \frac{d\bar{v}}{d\bar{r}} \right| \phi^2 \frac{1}{\left(1 - \frac{\phi}{\phi_m}\right)^{-\beta} e^{-M\bar{\theta}} \left| \frac{d\bar{v}}{d\bar{r}} \right|^m} \frac{d}{d\bar{r}} \left[ \left(1 - \frac{\phi}{\phi_m}\right)^{-\beta} e^{-M\bar{\theta}} \left| \frac{d\bar{v}}{d\bar{r}} \right|^m \right] = 0 \end{aligned} \tag{32}$$

$$R_4 \left(1 - \frac{\phi}{\phi_m}\right)^{-\beta} e^{-M\bar{\theta}} \left| \frac{d\bar{v}}{d\bar{r}} \right|^{m+2} - \frac{1}{\bar{r}^2} \frac{d}{d\bar{r}} \left( \bar{r}^2 (1 + 3\zeta\phi + \xi\phi^2) \frac{d\bar{\theta}}{d\bar{r}} \right) = 0 \tag{33}$$

where  $R_4 = \frac{\mu_r V^2}{k_m (\theta_i - \theta_0)} \left(\frac{V}{R_o}\right)^m$ , and  $\frac{K_c}{K_\mu}$  is the ratio of the effect of varying interaction frequency to varying the viscosity on the non-uniform distribution of volume fraction. Substituting Equation (29) into Equations (27) and (28) gives:

$$\begin{cases} \text{at } \bar{r} = \frac{R_i}{R_o} : \bar{v} = 1; \bar{\theta} = 1. \\ \text{at } \bar{r} = 1 : \bar{v} = 0; \bar{\theta} = 0; \end{cases} \tag{34}$$

$$\phi_{avg} = \frac{2}{1 - R_i^2} \int_{\frac{R_i}{R_o}}^1 \phi r dr \tag{35}$$

Now Equations (30), (32) and (33) can be solved numerically with the conditions and constraints of Equations (34) and (35). Note that  $R_4$  is related to the Prandtl and Eckert numbers ( $R_4 = PrEc$ ).

### 5. Numerical Results

The dimensionless differential equations are solved using the MATLAB solver bvp4c, which is a collocation boundary value problem solver. The step size is automatically adjusted by the solver and the default relative tolerance for the maximum residue is 0.001. The constraint Equation (35) for  $\phi_{avg}$  was achieved by applying the shooting method. Table 1 shows the designated values of the studied dimensionless numbers and parameters in current work.

**Table 1.** Designated values of the dimensionless numbers and parameters.

<b>m</b>	$\phi_m$	<b>M</b>	$R_4$
−0.5, 0.0, 0.5, 1.0	0.45, 0.5, 0.68, 0.9	0.0, 0.5, 1.0, 5.0	0.1, 0.5, 2.0, 3.0
$\omega$	$K_c/K_\mu$	$\phi_{avg}$	–
0.01, 1.0, 100.0, 1000.0	0.4, 0.6, 0.8, 0.9	0.1, 0.3, 0.4, 0.6	–

#### 5.1. Effect of m

Figures 2–4 show the effect of m on the distribution of velocity, volume fraction and temperature. Recall that when  $m > 0$  the fluid is shear thickening and when  $m < 0$  the fluid is shear thinning. Therefore, we can see that as m increases, that is, as the fluid increasingly shear thickens, contributing to a more uniform apparent viscosity, the velocity profiles become more linear as shown in Figure 2. From Figure 3 we can see that the shear-dependent viscosity has a strong effect on the particle distribution. For the case when  $m = 1$ , the value of the volume fraction at the outer wall is about ten times that of the value of the volume fraction at the inner wall. For the range of parameters considered in this study we can see that the effect of m on the temperature distribution is very small.

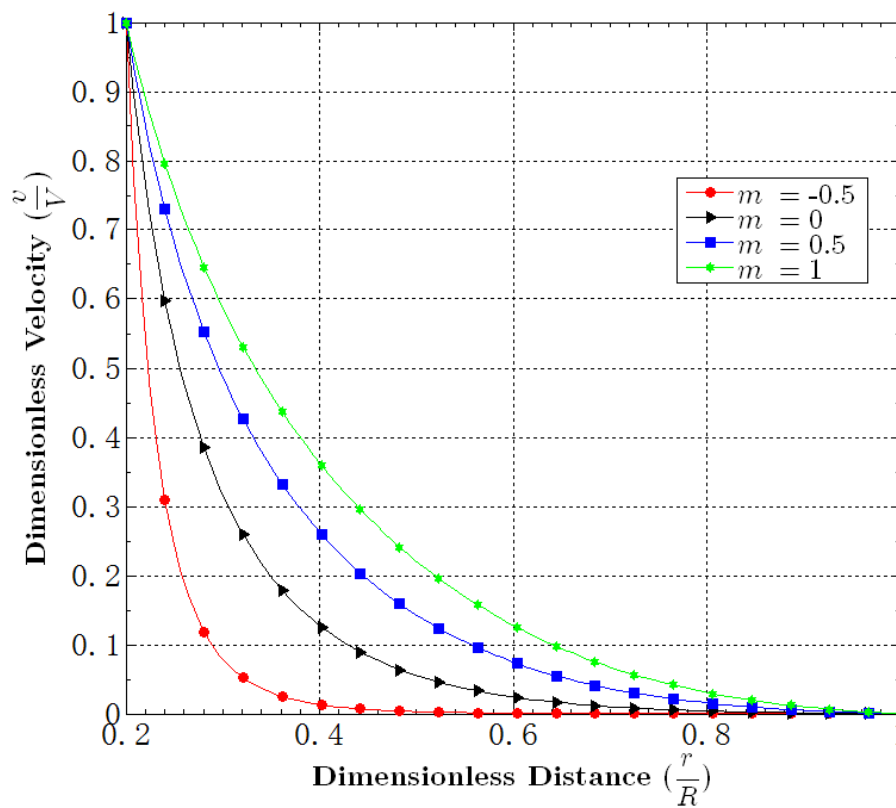


**Figure 2.** Effect of  $m$  on the velocity field when  $\phi_m = 0.68$ ,  $M = 1$ ,  $R_4 = 0.1$ ,  $\omega = 10$ ,  $K_c/K_\mu = 0.8$ ,  $\phi_{avg} = 0.4$ .

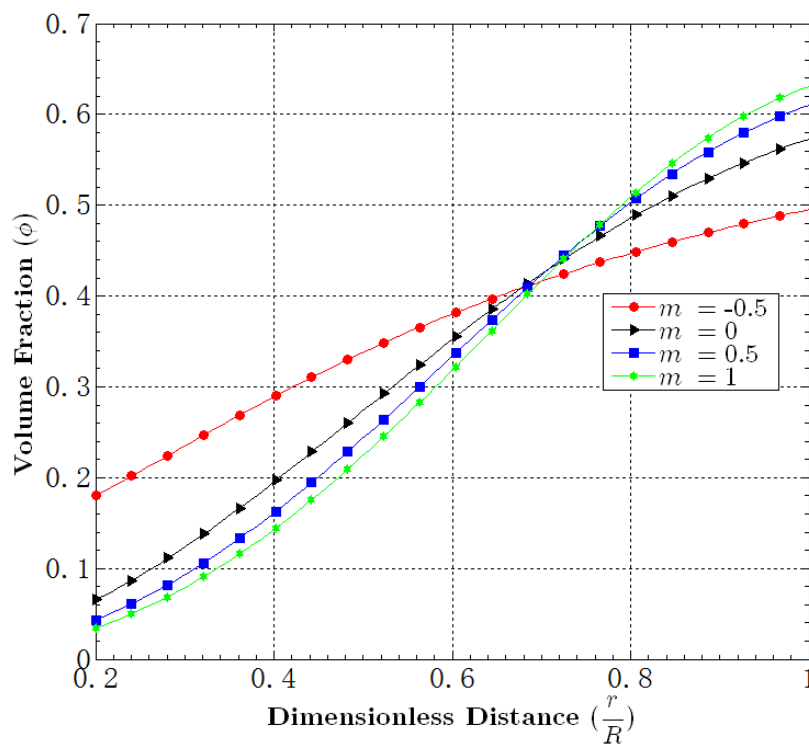


**Figure 3.** Effect of  $m$  on the volume fraction field when  $\phi_m = 0.68$ ,  $M = 1$ ,  $R_4 = 0.1$ ,  $\omega = 10$ ,  $K_c/K_\mu = 0.8$ ,  $\phi_{avg} = 0.4$ .

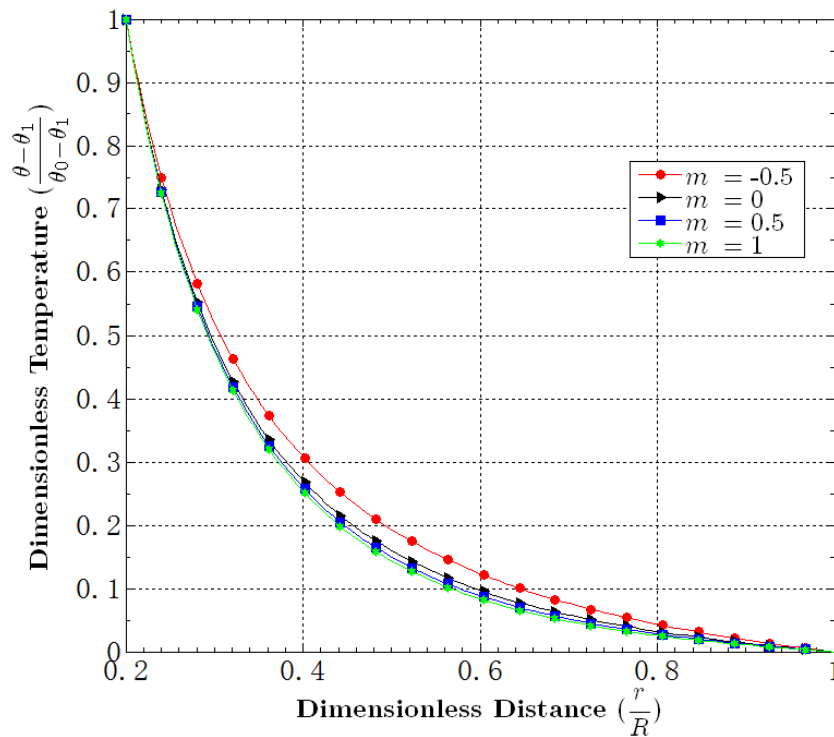


**Figure 4.** Effect of  $m$  on the temperature field when  $\phi_m = 0.68$ ,  $M = 1$ ,  $R_4 = 0.1$ ,  $\omega = 10$ ,  $K_c/K_\mu = 0.8$ ,  $\phi_{avg} = 0.4$ .

5.2. Effect of  $\phi_m$

Recall that  $\phi_m$  represents the maximum packing of solid particles in a solid-fluid system. A higher maximum packing can be attributed to the non-uniform distribution of the particle sizes, the deformability of the particles and so on. From Figure 5 we can see that a smaller  $\phi_m$  produces a more non-linear velocity profile. Figure 6 shows that as  $\phi_m$  increases, the volume fraction distribution becomes more non-uniform. For the case of  $\phi_m = 0.45$ , it can be seen that near the outer wall, the particle distribution is very uniform and the value of the volume fraction is close to 0.45. Furthermore, in that region, the fluid motion is negligible (see Figure 5). In other words, the particles seem to accumulate in the region near the outer wall. Similar to the parameter  $m$ , the effect of  $\phi_m$  on temperature distribution is negligible (see Figure 7).

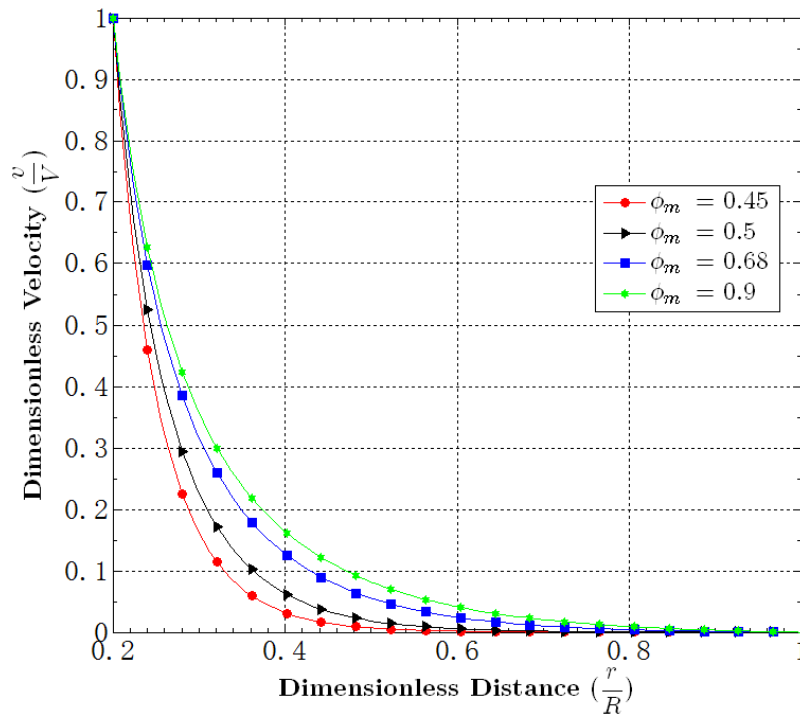


**Figure 5.** Effect of  $\phi_m$  on the velocity field when  $m = 0.0$ ,  $M = 1$ ,  $R_4 = 0.1$ ,  $\omega = 10$ ,  $K_c/K_\mu = 0.8$ ,  $\phi_{avg} = 0.4$ .

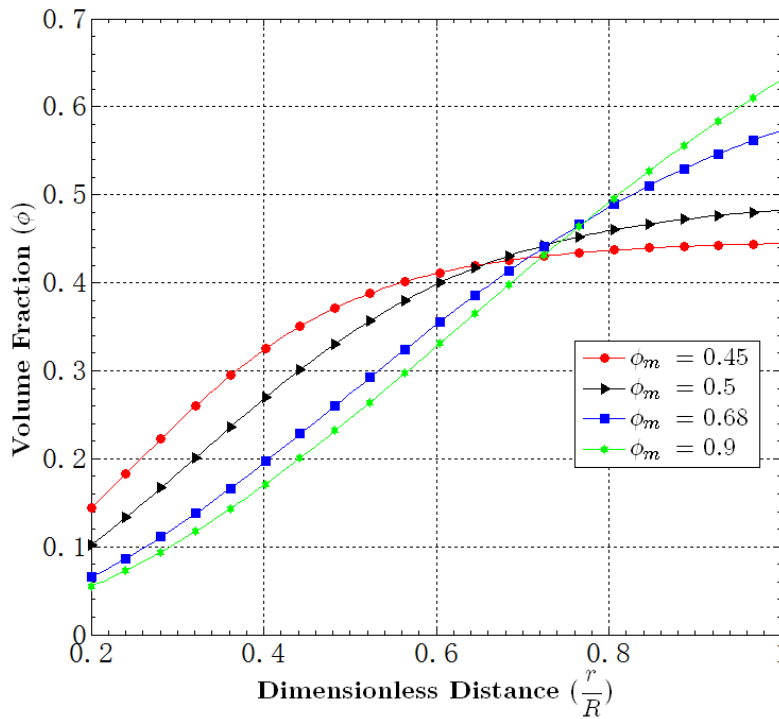


**Figure 6.** Effect of  $\phi_m$  on the volume fraction field when  $m = 0.0$ ,  $M = 1$ ,  $R_4 = 0.1$ ,  $\omega = 10$ ,  $K_c/K_\mu = 0.8$ ,  $\phi_{avg} = 0.4$ .

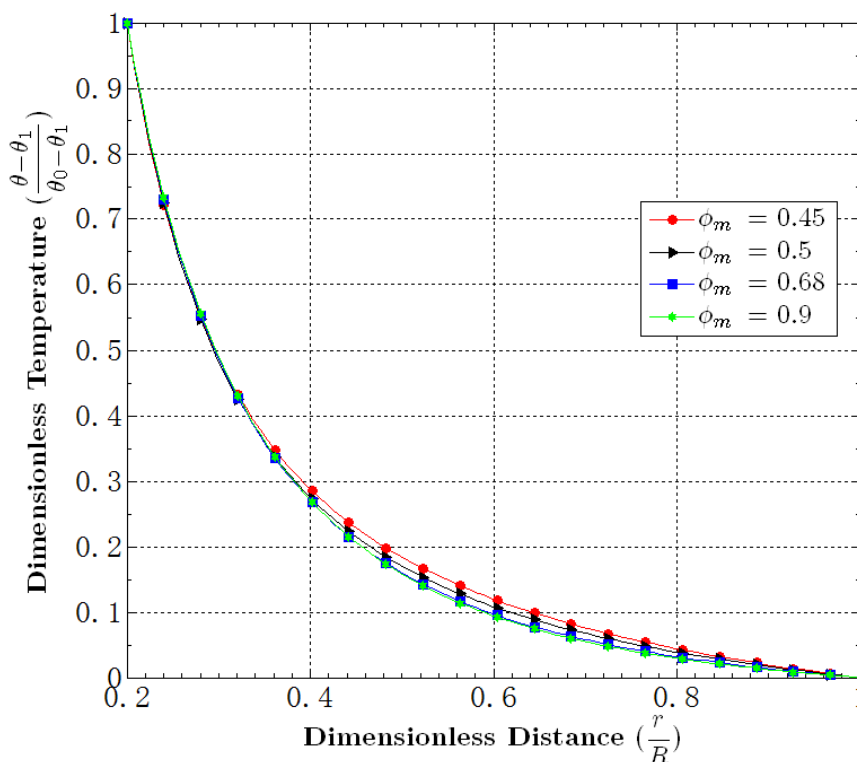


**Figure 7.** Effect of  $\phi_m$  on the temperature field when  $m = 0.0$ ,  $M = 1$ ,  $R_4 = 0.1$ ,  $\omega = 10$ ,  $K_c/K_\mu = 0.8$ ,  $\phi_{avg} = 0.4$ .

### 5.3. Effect of $M$

In the current model,  $M$  is the parameter controlling the effect of temperature on the apparent viscosity. A larger  $M$  represents a higher sensitivity of the viscosity on the temperature change. Therefore, from Figure 8, we can see that as  $M$  increases, the velocity curve becomes more non-linear, which can be attributed to a more non-linear behavior of the apparent viscosity. It should be emphasized that if we had considered a pressure-driven flow, then as  $M$  increases we would expect a higher flow rate, since with the same temperature, a larger  $M$  implies a lower apparent viscosity. Figure 8 shows that at a larger  $M$ , such as  $M = 5$ , a higher velocity is reached mainly in the region near the inner wall. From Figures 9 and 10 we can see that the effect of  $M$  on the volume fraction and temperature distribution is minimal.

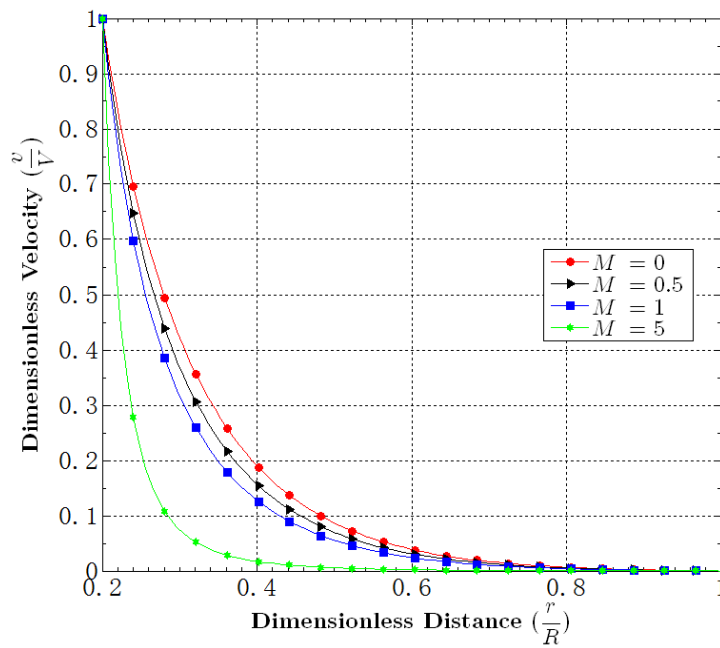


**Figure 8.** Effect of  $M$  on the velocity field when  $m = 0.0$ ,  $\phi_m = 0.68$ ,  $R_4 = 0.1$ ,  $\omega = 10$ ,  $K_c/K_\mu = 0.8$ ,  $\phi_{avg} = 0.4$ .

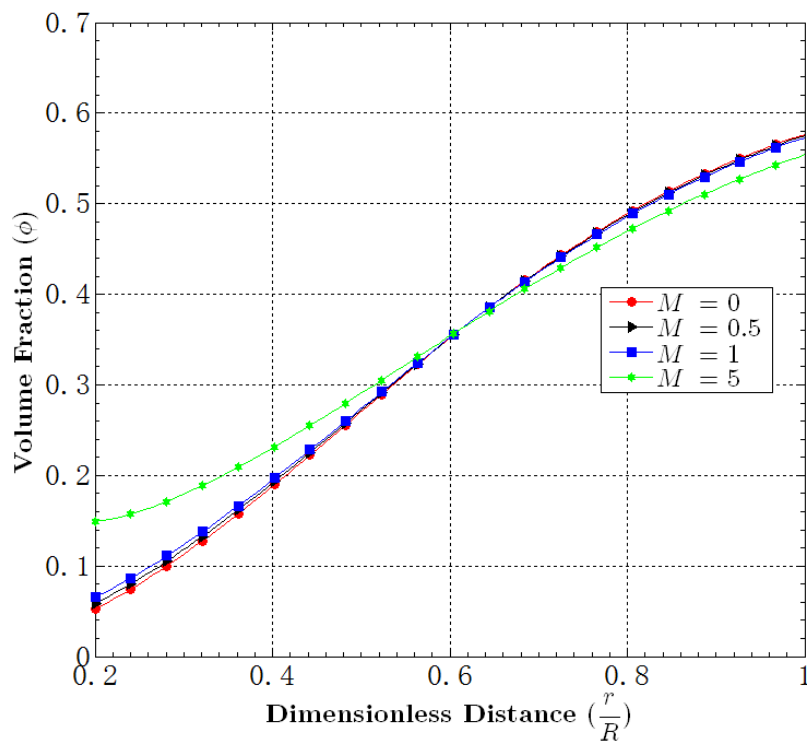


**Figure 9.** Effect of  $M$  on the volume fraction field when  $m = 0.0$ ,  $\phi_m = 0.68$ ,  $R_4 = 0.1$ ,  $\omega = 10$ ,  $K_c/K_\mu = 0.8$ ,  $\phi_{avg} = 0.4$ .

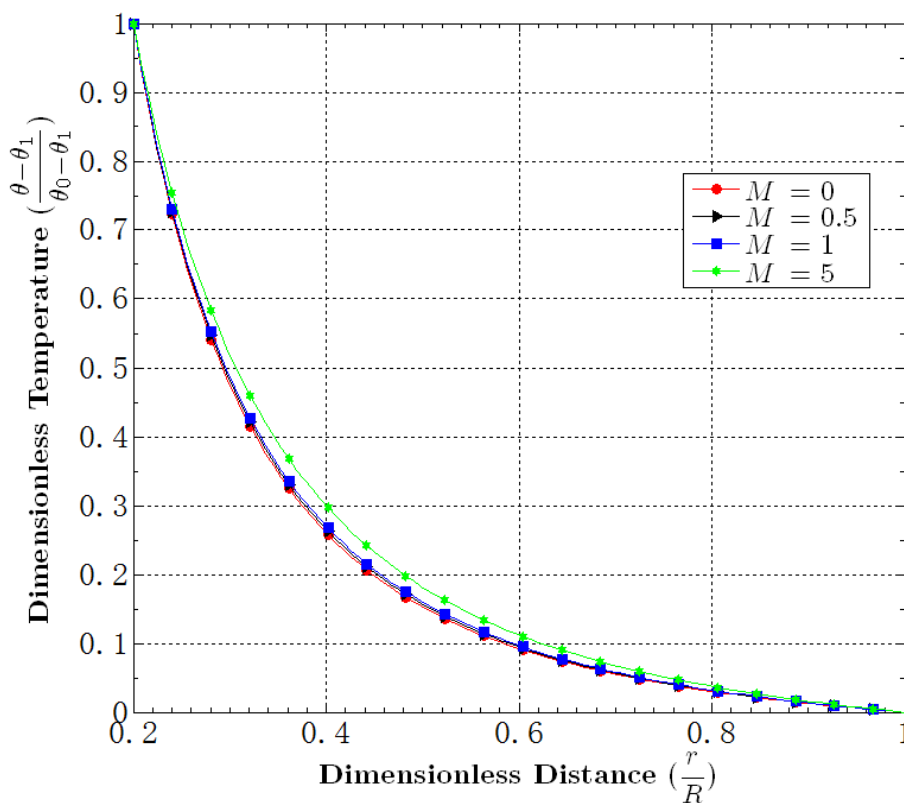


**Figure 10.** Effect of M on the temperature field when  $m = 0.0$ ,  $\phi_m = 0.68$ ,  $R_4 = 0.1$ ,  $\omega = 10$ ,  $K_c/K_\mu = 0.8$ ,  $\phi_{avg} = 0.4$ .

5.4. Effect of  $R_4$

Recall that  $R_4$  is defined as  $\frac{\mu_r V^2}{k_m (\theta_1 - \theta_0)} \left(\frac{V}{H}\right)^m$ , which is a measure of viscous dissipation and is related to the Prandtl and the Eckert numbers. Figures 11–13 show the impact of  $R_4$  in this problem. From Figures 11 and 12 it can be seen that the effect of  $R_4$  on the velocity and volume fraction distribution is negligible. From Figure 13 it can be seen that  $R_4$  increases if the temperature profiles become more non-linear. From the expression of  $R_4$ , we know that a larger  $R_4$  implies a stronger effect of the shear stress on temperature distribution; furthermore, from the velocity profile, we can see that near the inner wall, the velocity gradient is larger and therefore a larger  $R_4$  has the tendency to increase the temperature gradient near the inner wall region.

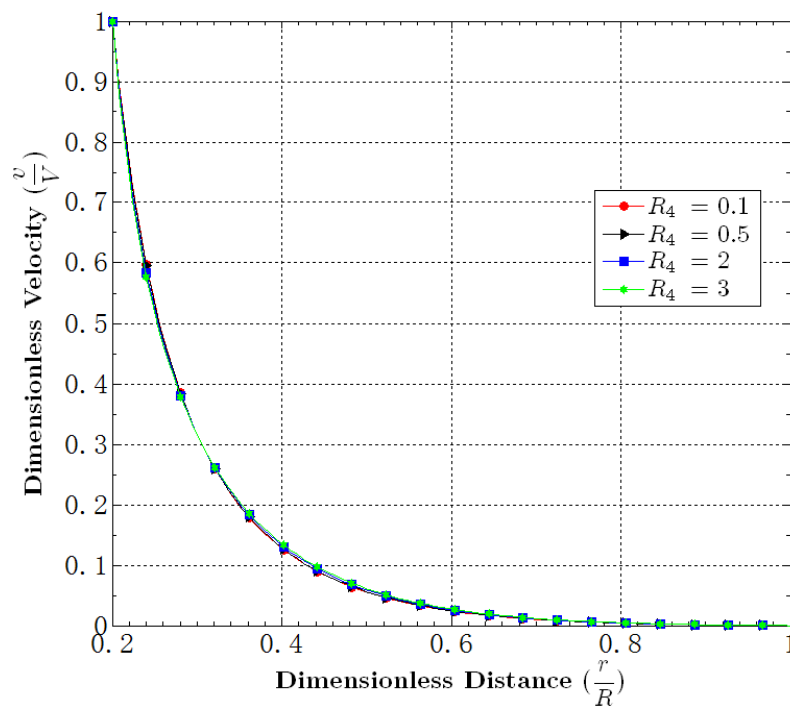


**Figure 11.** Effect of  $R_4$  on the velocity field when  $m = 0.0$ ,  $\phi_m = 0.68$ ,  $M = 1$ ,  $\omega = 10$ ,  $K_c/K_\mu = 0.8$ ,  $\phi_{avg} = 0.4$ .

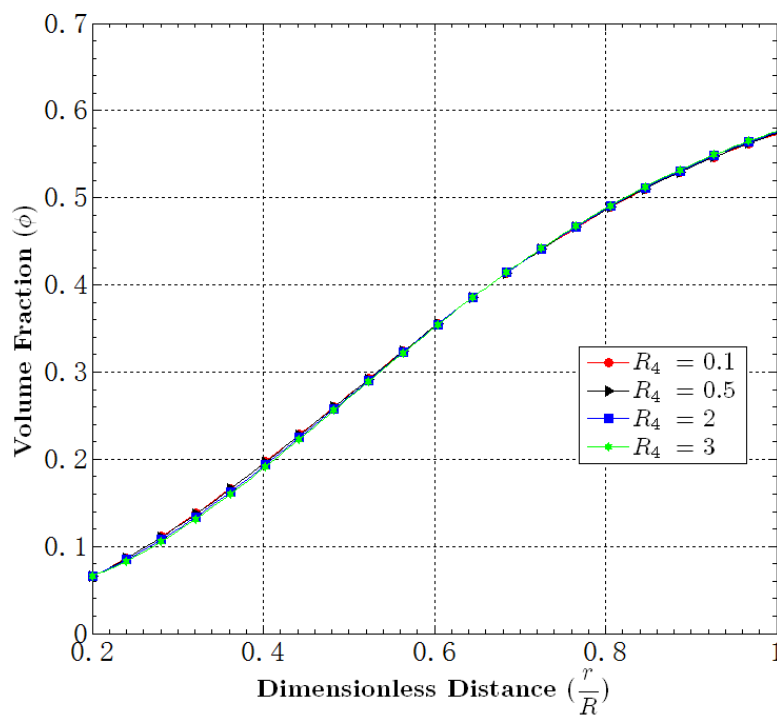


**Figure 12.** Effect of  $R_4$  on the volume fraction field when  $m = 0.0$ ,  $\phi_m = 0.68$ ,  $M = 1$ ,  $\omega = 10$ ,  $K_c/K_\mu = 0.8$ ,  $\phi_{avg} = 0.4$ .

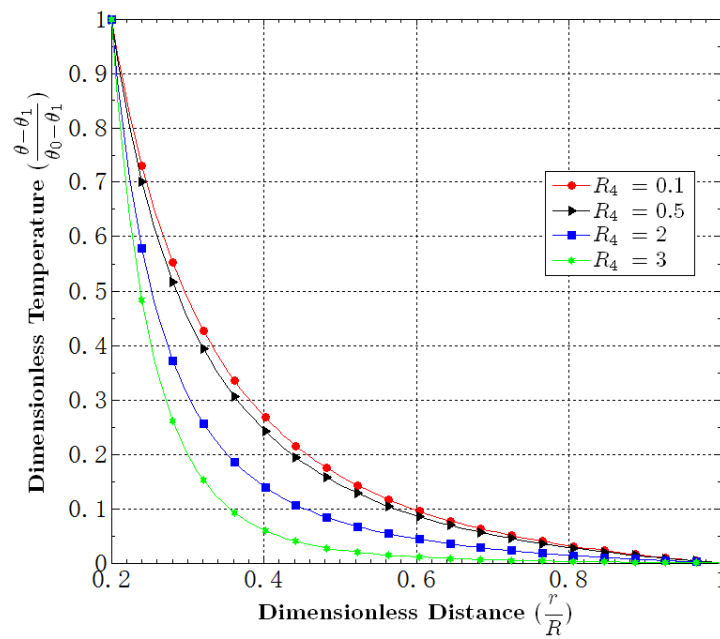


**Figure 13.** Effect of  $R_4$  on the temperature field when  $m = 0.0$ ,  $\phi_m = 0.68$ ,  $M = 1$ ,  $\omega = 10$ ,  $K_c/K_\mu = 0.8$ ,  $\phi_{avg} = 0.4$ .

5.5. Effect of  $\omega$

Recall that  $\omega$  represents the ratio of the conductivity of the particles to the matrix;  $\omega$  only appears in the energy equation. Therefore, as expected from Figures 14 and 15 we can see that the effect of  $\omega$  on the velocity and the volume fraction distribution is meagre. Figure 16 shows the effect of  $\omega$  on the temperature profile. It can be seen that as  $\omega$  increases, the temperature distribution becomes more non-linear. This may be attributed to the higher dependency of the thermal conductivity on the volume fraction as  $\omega$  increases.

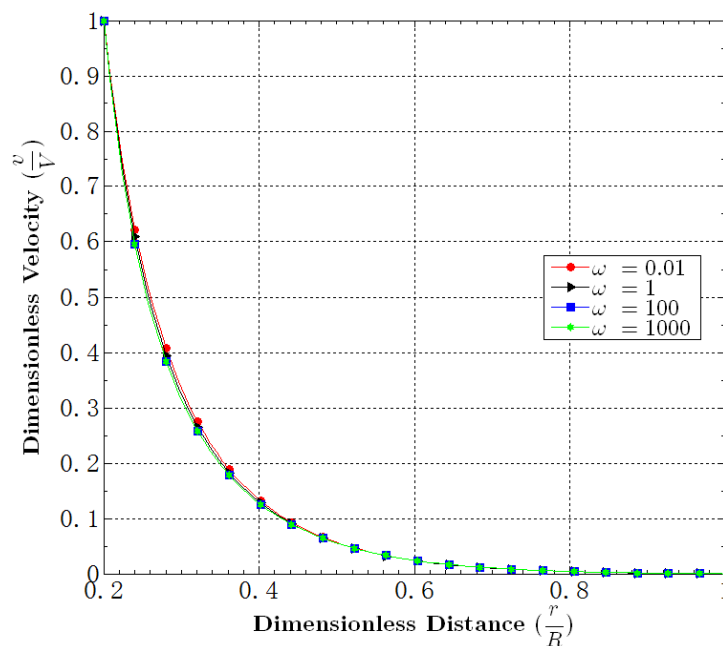


**Figure 14.** Effect of  $\omega$  on the velocity field when  $m = 0.0$ ,  $\phi_m = 0.68$ ,  $M = 1$ ,  $R_4 = 0.1$ ,  $K_c/K_\mu = 0.8$ ,  $\phi_{avg} = 0.4$ .

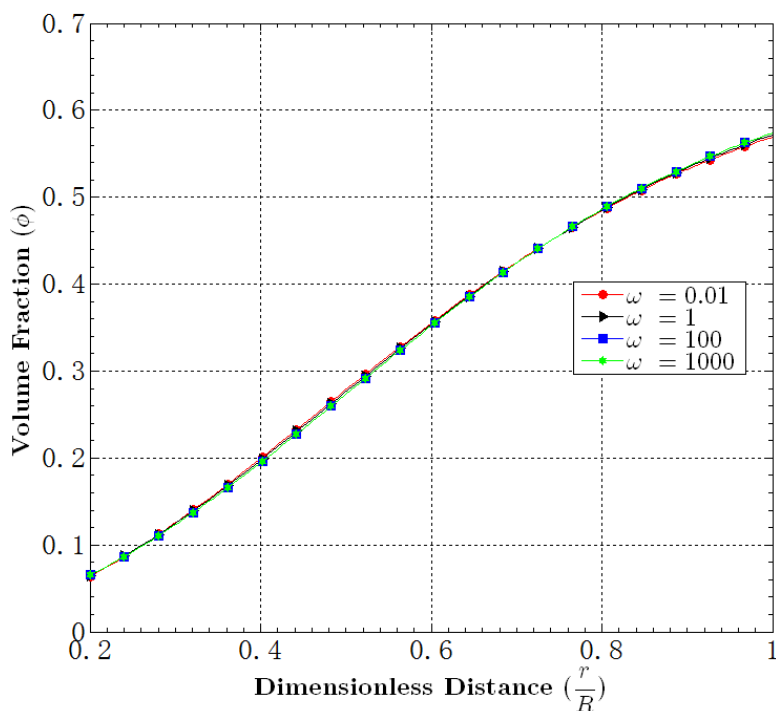


**Figure 15.** Effect of  $\omega$  on the volume fraction field when  $m = 0.0$ ,  $\phi_m = 0.68$ ,  $M = 1$ ,  $R_4 = 0.1$ ,  $K_c/K_\mu = 0.8$ ,  $\phi_{avg} = 0.4$ .

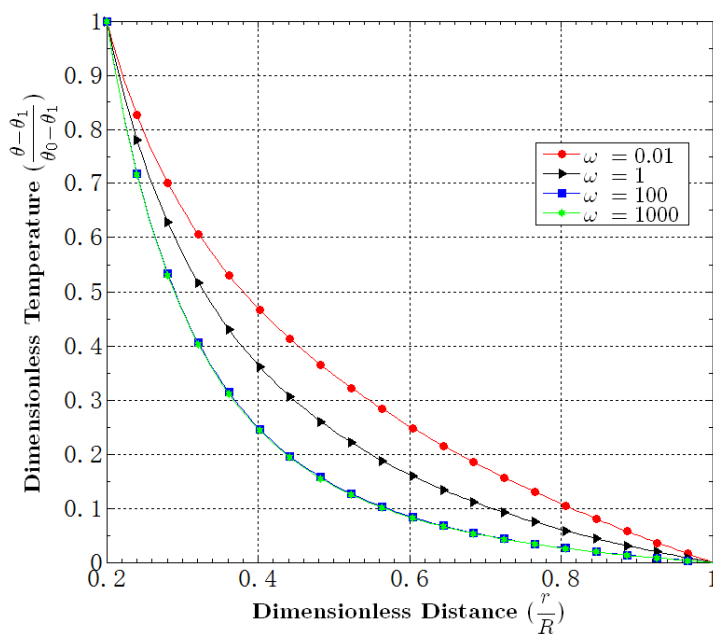


**Figure 16.** Effect of  $\omega$  on the temperature field when  $m = 0.0$ ,  $\phi_m = 0.68$ ,  $M = 1$ ,  $R_4 = 0.1$ ,  $K_c/K_\mu = 0.8$ ,  $\phi_{avg} = 0.4$ .

5.6. Effect of  $K_c/K_\mu$

Figures 17–19 show the effect of  $K_c/K_\mu$ . This ratio represents the effect of varying interaction frequency to varying viscosity on the non-uniform distribution of the volume fraction. From Figure 18, we can see that as  $K_c/K_\mu$  decreases, the particle distribution becomes more uniform. That is, when the  $K_c/K_\mu$  is small, a small particle non-uniformity can cause viscosity gradients large enough to satisfy

Equation (32) [17]. Figures 17 and 19 show that as  $K_c/K_\mu$  increases, the velocity and the temperature curves become more linear, though the effect is small.

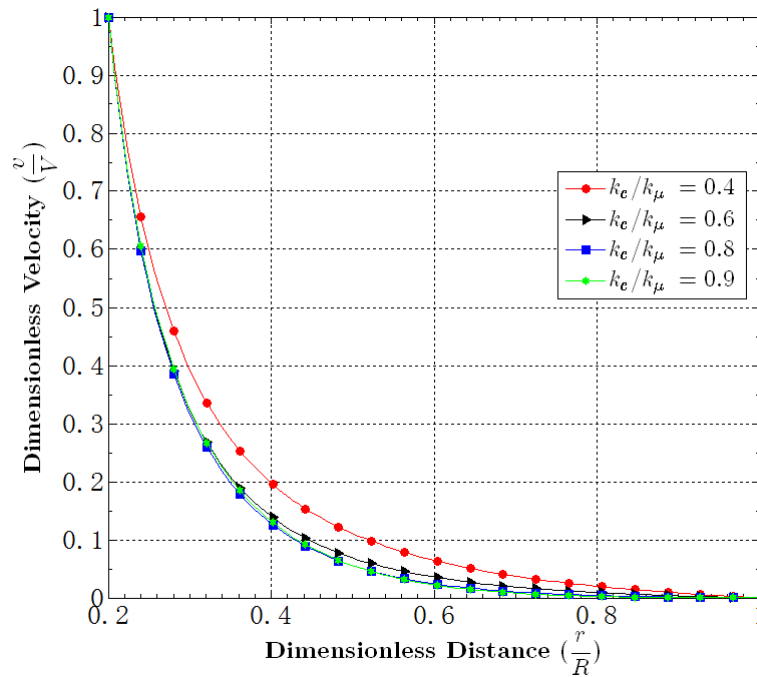


**Figure 17.** Effect of  $K_c/K_\mu$  on the velocity field when  $m = 0.0$ ,  $\phi_m = 0.68$ ,  $M = 1$ ,  $R_4 = 0.1$ ,  $\omega = 10$ ,  $\phi_{avg} = 0.4$ .

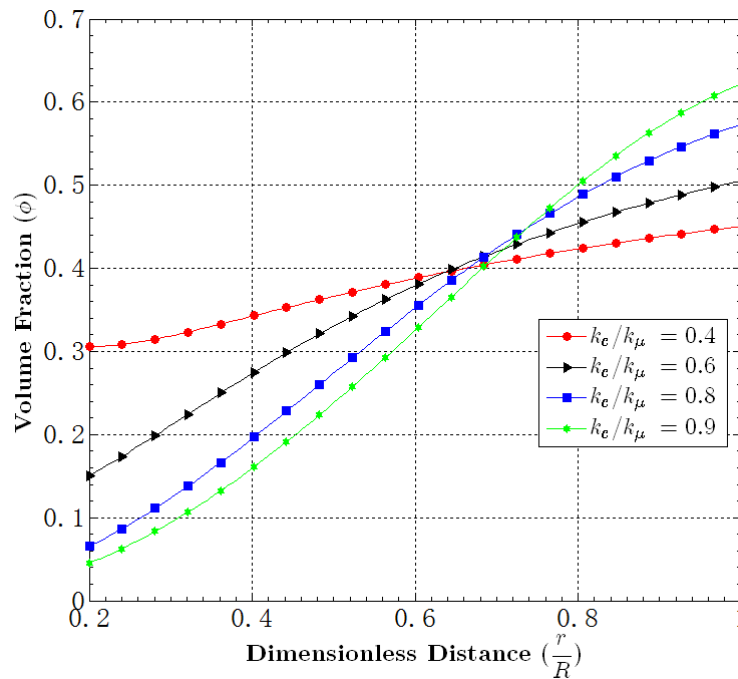


**Figure 18.** Effect of  $K_c/K_\mu$  on the volume fraction field when  $m = 0.0$ ,  $\phi_m = 0.68$ ,  $M = 1$ ,  $R_4 = 0.1$ ,  $\omega = 10$ ,  $\phi_{avg} = 0.4$ .

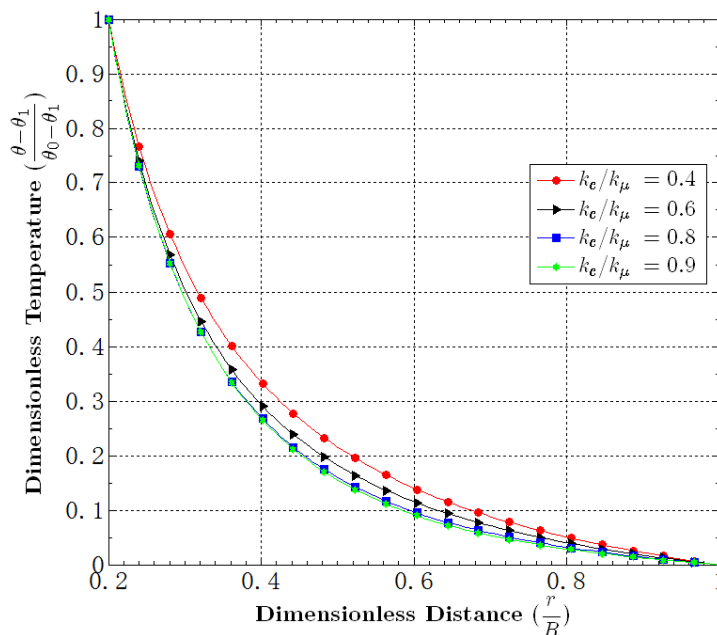


**Figure 19.** Effect of  $K_c/K_\mu$  on the temperature field when  $m = 0.0$ ,  $\phi_m = 0.68$ ,  $M = 1$ ,  $R_4 = 0.1$ ,  $\omega = 10$ ,  $\phi_{avg} = 0.4$ .

5.7. Effect of the Average Volume Fraction  $\phi_{avg}$

From Figure 20, it can be seen that when  $\phi_{avg}$  increases, the velocity curves become more non-linear. This may be attributed to higher non-uniform distribution of volume fraction when  $\phi_{avg}$  is high. As Figure 21 shows, the effect of  $\phi_{avg}$  on the volume fraction distribution is strong. For higher values of  $\phi_{avg}$ , the volume fraction profile becomes more non-linear; that is, more particles stack near the outer wall. At the same time, we can see that the velocity does not change much in the region where the particles accumulate. That is as expected, since when the bulk volume fraction is approaching the maximum packing, then a very high apparent viscosity is reached. From Figure 22, we can see that the effect of  $\phi_{avg}$  on temperature profile is negligible.

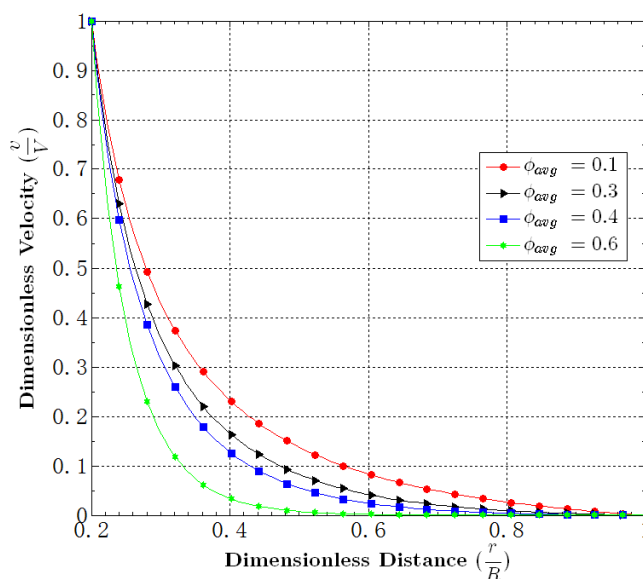


**Figure 20.** Effect of  $\phi_{avg}$  on the velocity field when  $m = 0.0$ ,  $\phi_m = 0.68$ ,  $M = 1$ ,  $R_4 = 0.1$ ,  $\omega = 10$ ,  $K_c/K_\mu = 0.8$ .

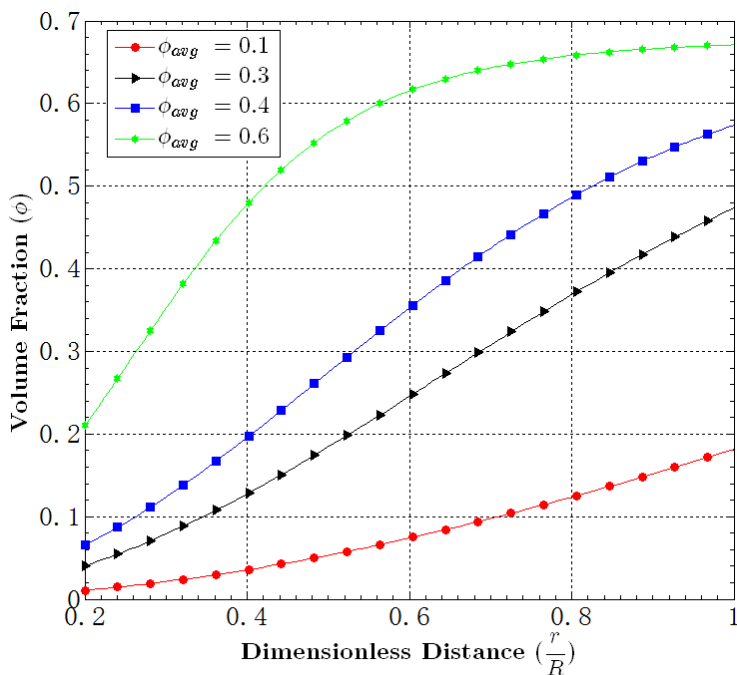


**Figure 21.** Effect of  $\phi_{avg}$  on the volume fraction field when  $m = 0.0$ ,  $\phi_m = 0.68$ ,  $M = 1$ ,  $R_4 = 0.1$ ,  $\omega = 10$ ,  $K_c/K_\mu = 0.8$ .

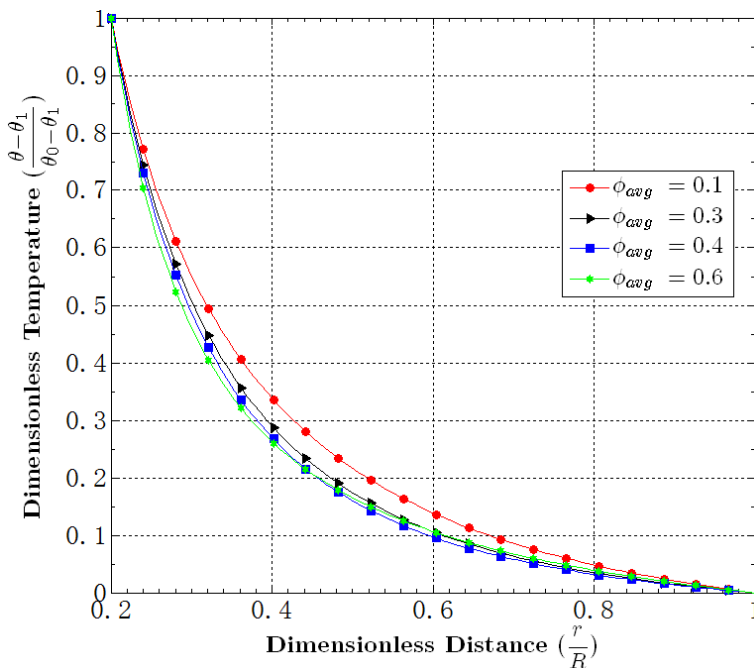


**Figure 22.** Effect of  $\phi_{avg}$  on the temperature field when  $m = 0.0$ ,  $\phi_m = 0.68$ ,  $M = 1$ ,  $R_4 = 0.1$ ,  $\omega = 10$ ,  $K_c/K_\mu = 0.8$ .

### 6. Concluding Remarks

In this paper, we have studied the fully developed flow of a drilling fluid between two rotating cylinders. We have modeled the drilling fluid as a non-Newtonian suspension. The viscosity is assumed to depend not only on the volume fraction and the shear rate but also on the temperature. To study the variation of the volume fraction, a convection-diffusion equation with a concentration

flux suggested by Phillips *et al.* [17] is used. The condition of the fully developed flow is considered and the governing equations are non-dimensionalized and numerically solved. The parametric study indicates that the flow field is greatly affected by the dependency of the viscosity on the shear rate and the temperature, and that the concentration flux parameters,  $K_c/K_\mu$ , and the solid-particle maximum packing,  $\phi_m$ , play a significant role in the particle distribution. For future studies, we plan to consider the yield stress portion of the stress tensor, as well as look at unsteady multi-dimensional flow situations. Furthermore, the effects of viscous dissipation near the tip of the drilling bit is considered to be more significant than inside the flow domain, and therefore, we plan to study the torsional and longitudinal oscillation of a cylindrical rod immersed in a non-linear fluid.

**Author Contributions:** Both authors contributed to the writing of the paper. Most of the mathematical formulation was primarily done by Mehrdad Massoudi, part of the derivation and all of the numerical work were done by Wei-Tao Wu.

**Conflicts of Interest:** The authors declare no conflict of interest.

## Nomenclature

Symbol	Explanation
$\mathbf{b}$	body force vector
$\phi$	concentration
$\mathbf{D}$	symmetric part of the velocity gradient
$\mathbf{g}$	acceleration due to gravity
$\mathbf{I}$	identity tensor
$\mathbf{L}$	gradient of the velocity vector
$m$	Power-law index
$t$	time
$\mathbf{T}$	Cauchy stress tensor
$\rho$	bulk density
$\mu_r$	reference viscosity
$\eta$	effective viscosity
$\theta$	temperature
div	divergence operator
$\nabla$ (or grad)	gradient operator

## References

- Joseph, D.; Renardy, Y. Fundamentals of two-fluid dynamics. *J. Fluid Mech.* **1995**, *282*, 405–406.
- Rajagopal, K.; Tao, L. *Mechanics of Mixtures*; Series on Advances in Mathematics for Applied Sciences; World Scientific: Singapore, 1995; Volume 35.
- Zhou, Z.; Wu, W.-T.; Massoudi, M. Fully developed flow of a drilling fluid between two rotating cylinders. *Appl. Math. Comput.* **2016**, *281*, 266–277. [[CrossRef](#)]
- Gray, G.R.; Darley, H. *Composition and Properties of Oilwell Drilling Fluids*; Gulf Publishing Company: London, UK, 1981.
- Rabia, H. *Oilwell Drilling Engineering: Principles and Practice*; Graham and Trotman Ltd: London, UK, 1985.
- Caenn, R.; Chillingar, G.V. Drilling fluids: State of the art. *J. Pet. Sci. Eng.* **1996**, *14*, 221–230. [[CrossRef](#)]
- Siginer, D.A.; Bakhtiyarov, S.I. Flow of drilling fluids in eccentric annuli. *J. Non-Newton. Fluid Mech.* **1998**, *78*, 119–132. [[CrossRef](#)]
- Fam, M.A.; Dusseault, M.B.; Fooks, J.C. Drilling in mudrocks: Rock behavior issues. *J. Pet. Sci. Eng.* **2003**, *38*, 155–166. [[CrossRef](#)]
- Valluri, S.G.; Miska, S.Z.; Yu, M.; Ahmed, R.M.; Takach, N. Experimental study of effective hole cleaning using “sweeps” in horizontal wellbores. In Proceedings of the SPE Annual Technical Conference and Exhibition, San Antonio, TX, USA, 24–27 September 2006.
- Coussot, P. *Mudflow Rheology and Dynamics*; Balkema: Amsterdam, The Netherlands, 1997.

11. Yield-power Law Model More Accurately Predicts Mud Rheology. Available online: <http://www.ogj.com/articles/print/volume-91/issue-34/in-this-issue/drilling/yield-power-law-model-more-accurately-predicts-mud-rheology.html> (accessed on 17 March 2016).
12. Sławomirski, M.R. Rheological behavior of oil well drilling fluids. *Int. J. Rock Mech. Min. Sci. Geomech. Abstr.* **1975**, *12*, 115–123. [[CrossRef](#)]
13. Briscoe, B.; Luckham, P.; Ren, S. The properties of drilling muds at high pressures and high temperatures. *Philos. Trans. R. Soc. Lond. A Math. Phys. Eng. Sci.* **1994**, *348*, 179–207. [[CrossRef](#)]
14. Massoudi, M. A mixture theory formulation for hydraulic or pneumatic transport of solid particles. *Int. J. Eng. Sci.* **2010**, *48*, 1440–1461. [[CrossRef](#)]
15. Massoudi, M. A note on the meaning of mixture viscosity using the classical continuum theories of mixtures. *Int. J. Eng. Sci.* **2008**, *46*, 677–689. [[CrossRef](#)]
16. Subia, S.R.; Ingber, M.S.; Mondy, L.A.; Altobelli, S.A.; Graham, A.L. Modelling of concentrated suspensions using a continuum constitutive equation. *J. Fluid Mech.* **1998**, *373*, 193–219. [[CrossRef](#)]
17. Phillips, R.J.; Armstrong, R.C.; Brown, R.A.; Graham, A.L.; Abbott, J.R. A constitutive equation for concentrated suspensions that accounts for shear-induced particle migration. *Phys. Fluids A Fluid Dyn. (1989–1993)* **1992**, *4*, 30–40. [[CrossRef](#)]
18. Liu, I.-S. *Continuum Mechanics*; Springer: Berlin, Germany, 2002.
19. Müller, I. On the entropy inequality. *Arch. Ration. Mech. Anal.* **1967**, *26*, 118–141. [[CrossRef](#)]
20. Ziegler, H. *An Introduction to Thermomechanics*; North-Holland Publishing Company: Amsterdam, The Netherlands, 1983.
21. Truesdell, C.; Noll, W. *The Nonlinear Field Theories of Mechanics*; Springer-Verlag: Berlin, Germany, 1992.
22. Massoudi, M.; Wang, P. Slag behavior in gasifiers. Part II: Constitutive modeling of slag. *Energies* **2013**, *6*, 807–838. [[CrossRef](#)]
23. Gupta, G.; Massoudi, M. Flow of a generalized second grade fluid between heated plates. *Acta Mech.* **1993**, *99*, 21–33. [[CrossRef](#)]
24. Miao, L.; Wu, W.-T.; Aubry, N.; Massoudi, M. Heat transfer and flow of a slag-type non-linear fluid: Effects of variable thermal conductivity. *Appl. Math. Comput.* **2014**, *227*, 77–91. [[CrossRef](#)]
25. Miao, L.; Massoudi, M. Heat transfer analysis and flow of a slag-type fluid: Effects of variable thermal conductivity and viscosity. *Int. J. Non-Linear Mech.* **2015**, *76*, 8–19. [[CrossRef](#)]
26. Krieger, I.M. Rheology of monodisperse latices. *Adv. Colloid Interface Sci.* **1972**, *3*, 111–136. [[CrossRef](#)]
27. Roscoe, R. The viscosity of suspensions of rigid spheres. *Br. J. Appl. Phys.* **1952**, *3*, 267–269. [[CrossRef](#)]
28. Roscoe, R. *Flow Properties of Disperse Systems*; Hermans, J., Ed.; Interscience Publishers: New York, NY, USA, 1953; pp. 1–38.
29. Massoudi, M.; Vaidya, A. Unsteady flows of inhomogeneous incompressible fluids. *Int. J. Non-Linear Mech.* **2011**, *46*, 738–741. [[CrossRef](#)]
30. Massoudi, M.; Vaidya, A. Analytical solutions to stokes-type flows of inhomogeneous fluids. *Appl. Math. Comput.* **2012**, *218*, 6314–6329. [[CrossRef](#)]
31. Fourier, J. *The Analytical Theory of Heat*; Dover Publications: New York, NY, USA, 1955.
32. Winterton, R.H. Early study of heat transfer: Newton and fourier. *Heat Transf. Eng.* **2001**, *22*, 3–11. [[CrossRef](#)]
33. Kaviany, M. *Principles of Heat Transfer in Porous Media*; Springer: Berlin, Germany, 1995.
34. Bashir, Y.; Goddard, J. Experiments on the conductivity of suspensions of ionically-conductive spheres. *AIChE J.* **1990**, *36*, 387–396. [[CrossRef](#)]
35. Prasher, R.S.; Koning, P.; Shipley, J.; Devpura, A. Dependence of thermal conductivity and mechanical rigidity of particle-laden polymeric thermal interface material on particle volume fraction. *J. Electron. Packag.* **2003**, *125*, 386–391. [[CrossRef](#)]
36. Lee, D.-L.; Irvine, T.F., Jr. Shear rate dependent thermal conductivity measurements of non-newtonian fluids. *Exp. Therm. Fluid Sci.* **1997**, *15*, 16–24. [[CrossRef](#)]
37. Jeffrey, D.J. Conduction through a random suspension of spheres. *Proc. R. Soc. Lond. A Math. Phys. Sci.* **1973**, *335*, 355–367. [[CrossRef](#)]
38. Batchelor, G.; O'Brien, R. Thermal or electrical conduction through a granular material. *Proc. R. Soc. Lond. A Math. Phys. Sci.* **1977**, *355*, 313–333. [[CrossRef](#)]
39. Pabst, W. Simple second-order expression: For the porosity dependence of thermal conductivity. *J. Mater. Sci.* **2005**, *40*, 2667–2669. [[CrossRef](#)]

40. Miao, L.; Wu, W.T.; Aubry, N.; Massoudi, M. Falling film flow of a viscoelastic fluid along a wall. *Math. Methods Appl. Sci.* **2014**, *37*, 2840–2853. [[CrossRef](#)]
41. Massoudi, M.; Christie, I. Effects of variable viscosity and viscous dissipation on the flow of a third grade fluid in a pipe. *Int. J. Non-Linear Mech.* **1995**, *30*, 687–699. [[CrossRef](#)]



© 2016 by the authors; licensee MDPI, Basel, Switzerland. This article is an open access article distributed under the terms and conditions of the Creative Commons by Attribution (CC-BY) license (<http://creativecommons.org/licenses/by/4.0/>).